JOURNAL OF COMPUTATIONAL PHYSICS 41, 51–67 (1981)

PIC Calculations of Multiphase Flow*,†

THOMAS L. COOK, RUTH B. DEMUTH, AND FRANCIS H. HARLOW

Los Alamos Scientific Laboratory, Los Alamos, New Mexico 87545

Received October 31, 1979; revised March 31, 1980

The Particle-in-Cell method for the numerical solution of problems in fluid dynamics has been extended to the study of shock and rarefaction flows in a multiphase mixture. To test the numerical procedure, we have examined the propagation of sound signals through a mixture in which the theoretical speed is appreciably less than that of either material separately, with results that validate the calculational technique.

I. INTRODUCTION

Under several possible circumstances the passage of a shock across a density discontinuity can result in an instability of the interface followed by an interpenetration between the phases. One class of problems occurs when both materials are in a liquid or a vapor phase and the interface between them has had some perturbation impressed upon it. Another class occurs when one material is a liquid or a gas, and the other is a fragmented solid. In either case, instability and penetration take place only when the shock moves from the less dense to the more dense material. When both materials are in a liquid or vapor state, the process is closely related to the classical Rayleigh–Taylor instability of incompressible fluids.

When a shock passes through a liquid or a gas and impinges on a fragmented solid, the detailed dynamics are more complicated. The response of the solid depends on the extent of interpenetration by the driving gas at the contact surface. The interpenetration can be understood qualitatively in terms of the relative acceleration of material elements near the material interface as the shock first passes over. We illustrate this concept in Fig. 1. In Fig. 1a the shock is incident on the material interface from the low-density gas on the right. In Fig. 1b the acceleration of the fluid elements is shown after the passage of the shock. The lighter fluid elements have less inertia and consequently are accelerated more easily by the impulse. Under certain conditions, which we discuss quantitatively below, interpenetration results. The reverse situation is presented in Figs. 1c and d. The shock is incident from the left through the high-density material and the accelerations are in the opposite direction

† Work performed under the auspices of the U. S. Department of Energy.

0021-9991/81/050051-17$02.00/0

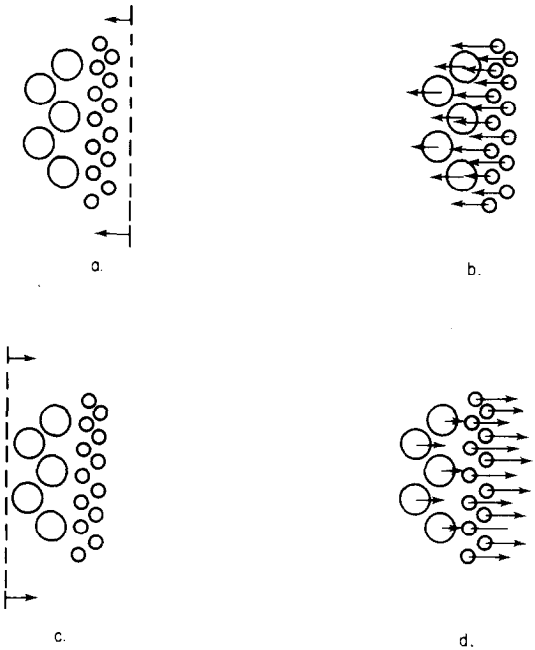

FIG. 1. Relative acceleration of material elements as a shock first passes over.

from those in Fig. 1b. The lighter fluid elements accelerate away from the heavier elements, no interpenetration occurs, and the contact surface remains sharply defined.

The methodology described below has been developed to study the problem of strong and weak shocks interacting with material interfaces. In particular we have examined the effects of shock passage across both leading and trailing edges of a fragmented metallic plate bounded on both sides by a gas of lighter density. The dynamic response of the plate depends on the severity of the instability that develops at the contact surface, and hence on the coupling between the two material fields. Details of this study are reported in Ref. [1].

Previous calculations of multiphase flow have been carried out in a completely Eulerian system [2]. For many purposes this type of representation is sufficiently accurate. In the present circumstances, however, there is one particular feature of the multiphase flow for which our preliminary calculations with a purely Eulerian representation are seriously deficient. Whereas most multiphase flow studies have emphasized the bulk interaction between already mixed phases, our present concern has been with the earliest stages of mix between phases in the vicinity of an interface that is initially sharp.

To illustrate the difficulty that can arise, we consider an initial configuration that consists of A, a region of pure gas, B, a region of fragmented metal, and C, another region of pure gas. The left wall is idealized as a rigid boundary, whereas the right wall is an inlet boundary through which a shock is introduced.

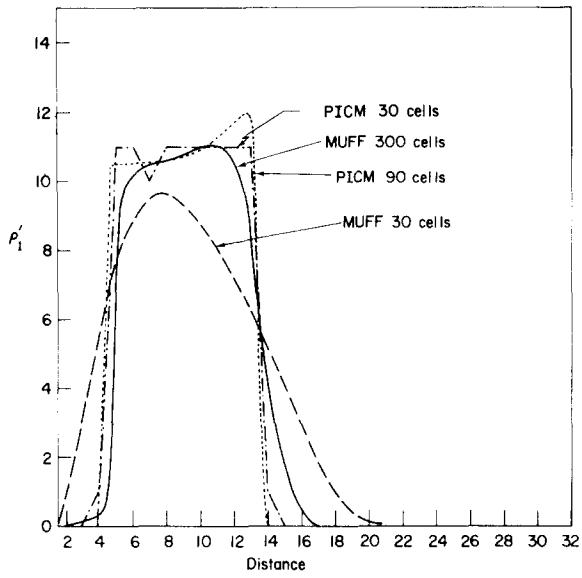

FIG. 2. Numerical diffusion: Macroscopic density of the metal predicted using coarse and fine Eulerian meshes and coarse and intermediate PICM meshes.

In Fig. 2 we plot the macroscopic density of a metallic disc that has been impacted by a strong shock. The disc is surrounded by a low-density gas. The shock travels from the right to the left; therefore the left contact surface is physically stable and any smearing is the result of numerical diffusion. The plots show that a purely Eulerian calculation performed with a code called MUFF (Multi-Fluid Flow) suffers from an intolerable level of numerical diffusion, even with very strong coupling between the two materials. It is easy to show that the diffusion extends over an effective distance that varies as the square root of the size of a computational cell. To reduce the diffusion to an acceptable level, however, would require cells very much smaller than those necessary for accurate resolution of the rest of the dynamics. To improve the accuracy of our solutions we have formulated a more elaborate scheme, based on the Particle-in-Cell (PIC) method [3]. This methodology is implemented in a computer code called PICM [1] (PIC Multi-phase). This new methodology allows the microscopic particles of the respective phases to cross over one another; hence it can be applied to multiphase situations where materials are interpenetrating.

II. The Differential Equations

The coupled differential equations and the exchange functions that describe the motion of a fluid composed of many materials, any one of which may be microscopically compressible or incompressible, are discussed in Ref. [3]. We

summarize below the one-dimensional, two-material, plane coordinate version of these equations.

Mass:

$$\frac{\partial \rho_l'}{\partial t} + \frac{\partial \rho_l' u_l}{\partial x} = 0. \tag{1}$$

where t is the time; x is the coordinate; ρ_l' is the macroscopic density of material l, that is, the total mass of l per unit total volume, and u_l is the velocity of l.

Momentum:

$$\rho_l' \frac{\partial u_l}{\partial t} + \rho_l' u_l \frac{\partial u_l}{\partial x} = -\theta_l \frac{\partial p}{\partial x} + V_l + K_{lm}(u_m - u_l). \tag{2}$$

The volume fraction of l is θ_l, the change in momentum of l from the action of artificial viscous forces is V_l, the drag function resulting from motion relative to material m is K_{lm}, and the pressure is p. It is postulated that the two materials are in local equilibrium, so we do not subscript p. We represent V_l by

$$V_l = -\frac{\partial q_l}{\partial x}, \tag{3}$$

where q_l is the artificial viscous stress. This stress is calculated by

$$q_l = -\rho_l' v_l \frac{\partial u_l}{\partial x}, \tag{4}$$

where v_l is the kinematic viscosity of l. The drag function [4], which controls the exchange of momentum between the materials, can be written in a simplified form for the case in which l is the dispersed phase (the fragmented metal) and m is the continuous phase (the gas).

$$K_{lm} = \frac{3}{8} \frac{C_D}{r_l} \theta_l \rho_m' |u_l - u_m|, \tag{5}$$

where C_D is the drag coefficient and r_l is the radius of a particle of l.

Energy:

$$\rho_l' \frac{\partial I_l}{\partial t} + \rho_l' u_l \frac{\partial I_l}{\partial x} = (\theta_l p + q_l) \frac{1}{\rho_l} \frac{d\rho_l}{dt} + \rho_l' K_{lm} \frac{(u_m - u_l)^2}{\rho_l' + \rho_m'} + \frac{\partial}{\partial x}\left(\rho_l' \xi_l \frac{\partial I_l}{\partial x}\right), \tag{6}$$

where I_l is the specific internal energy and ξ_l is the thermal conductivity. The equation of state of the materials completes the set. For this study we use the stiffened gas formulation,

$$p = a_l^2(\rho_l - \rho_{0l}) + (\gamma_l - 1)\rho_l I_l. \tag{7}$$

The microscopic density, ρ_l, is the mass of l per unit volume occupied by l, so that $\rho_l' = \theta_l \rho_l$. The parameters a_l, ρ_{0l}, and γ_l characterize the material.

III. Numerical Methodology

The basic procedure used in the PIC method can be qualitatively decribed in the following way. The spatial domain of interest is subdivided into a set of Eulerian computational cells. With each cell we associate such field variables as pressure, specific internal energy, and fluid velocity. In addition, we superimpose a Lagrangian set of marker particles. Each particle represents an element of fluid that moves through the Eulerian mesh and interacts with other elements of fluid in a procedure that couples the two materials together. The passage of time is divided into a sequence of computational cycles, each with duration δt. After specification of initial and boundary conditions the evolution of the configuration through time is accomplished by a prescribed set of calculational phases in each cycle. These phases can be summarized as follows.

Phase 1. An advancement of the field variables for each Eulerian cell is calculated as if both the particles and the cells follow the fluid motion. In this phase, therefore, no convective terms in the equations are calculated.

Phase 2. With the Eulerian cells returned to their original positions, the new particle coordinates are calculated and any resulting transport of a particle from one Eulerian cell to another is accompanied by calculations of the corresponding convection of mass, momentum, and energy.

Phase 3. The diffusion of heat is calculated.

The Eulerian calculational mesh and indexing scheme for a typical problem are shown in Fig. 3. Eulerian cell centers are identified by integers, interfaces by half-integers. The index $\bar{j}$ is the total number of interior cells. The indices j_1 and j_2 define regional interfaces. The three interior regions are initialized to contain either of two

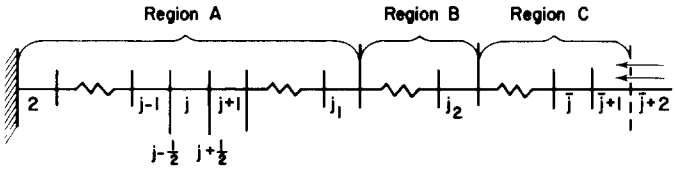

FIG. 3. The Eulerian calculational mesh for a typical problem.

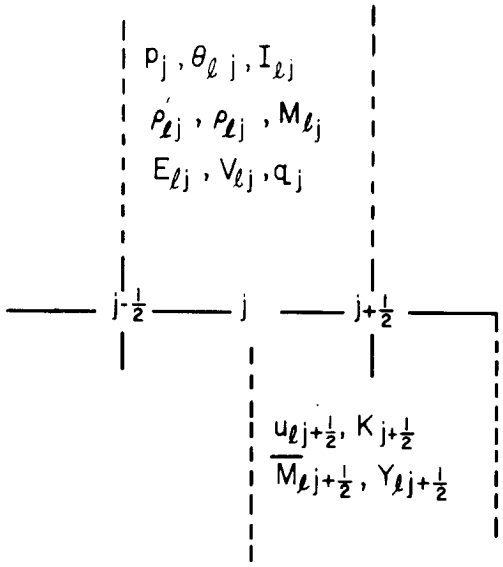

FIG. 4. Centering of the field variables.

materials or mixtures thereof. The left boundary is a rigid wall. At the right boundary we allow particles to be fluxed into the system from the exterior boundary cell according to prescribed conditions.

The Lagrangian particles are superimposed on this Eulerian mesh, their coordinates being denoted by the variable x_{lk}. The first subscript denotes the material; for this particular study, l is either 1 or 2. The second subscript identifies the particle. The initial number of particles of l in a cell is N_l. The total number of particles of l that are interior to the mesh is N_{l1}, whereas the total number of particles of l, including the particles held in reserve in the exterior boundary region, is N_{lT}.

As the system evolves through time, the Lagrangian particle distribution changes within the cells throughout the Eulerian mesh, determining the corresponding variations in the macroscopic fluid properties. The centering of the field variables is illustrated in Fig. 4. A complete set of variables must be specified for each material present. The first subscript identifies the material; the second subscript indicates the location of the variable. For two variables this categorization scheme is simplified. Since we assume pressure equilibrium between the materials, we drop the leading subscript for this variable and indicate only its location in the calculational mesh. The coupling coefficient K for a two-material system is likewise completely specified by indicating location. Pressure (p_j), volume fraction (θ_{lj}), specific internal energy (I_{lj}), macroscopic and microscopic densities (ρ'_{lj} and ρ_{lj}, where $\rho'_{lj} = \theta_{lj}\rho_{lj}$), total mass ($M_{lj}$), total internal energy (E_{lj}), cell volume (V_{lj}), and artificial viscous pressure (q_{lj}) are cell-centered quantities. Fluid velocity ($u_{lj+1/2}$), coupling coefficient between the fields ($K_{j+1/2}$), edge mass ($\bar{M}_{lj+1/2}$), and momentum ($Y_{lj+1/2}$) are interface variables.

Such cell-wise total quantities as mass M and volume V, are actually per unit cross-sectional area of the one-dimensional system. Previous calculations with the PIC method have treated the components of fluid velocity as cell-centered quantities. In anticipation of the development of an implicit version (see Ref. [1]) we have used cell-edge velocities in the present code.

In specifying initial conditions we choose the macroscopic fluid variables so that they represent the problem of interest. Consider the case in which region A is a pure gas, region B is fragmented metal, and region C is the same gas as region A. The right wall serves as an inlet boundary for an infinite-strength shock. We choose the initial densities of the fragmented metal disc and of the gas, which together with the Eulerian zone size, determine the total mass initially in every cell. We also set the pressures and the specific internal energies to their prescribed values everywhere in the interior. To initiate a problem, we select a rate u_{2R} at which the particles are to be fluxed in through the right boundary. The pressure, density, and specific internal energy in the right boundary cell are then determined by the Rankine–Hugoniot equations [5].

In addition to initializing the field variables, we must arrange the initial particle distribution in a manner consistent with the prescribed fluid properties. The mass m_l of every particle of a given material, wherever it appears in the system, is the same as the mass of every other particle of that same material. This mass is given by

$$m_l = \rho_l' \delta x / N_l, \tag{8}$$

where ρ_l' is the initial density in a region with particle density N_l, and δx is the Eulerian cell dimension. We define an initial particle spacing for each region shown in Fig. 3 by dividing the Eulerian cell dimension by the initial particle density of the appropriate material. The particle coordinates are initialized by uniformly distributing the mass within each phase throughout the appropriate material regions of the Eulerian mesh. The number of particles that must be held in reserve to feed the input shock at the right-hand boundary is

$$N_R = \frac{|u_{2R}|\, T_f}{\delta x} \frac{\rho_{2R}'}{\rho_{2C}'} N_2, \tag{9}$$

where N_R is the number of particles held in reserve, T_f is the total projected time over which the particles are to be injected, and ρ_{2R}'/ρ_{2C}' is the ratio of densities behind and in front of the input shock.

The initial conditions are not limited to the circumstances described by the above example; any other set of pure or mixed regions can be created, with whatever degree of inhomogeneity desired.

In phase 1 of the calculations we advance the field variables as if both the particles and the cells follow the fluid motion. Left superscripts count the time cycle. The new cell volumes $\tilde{V}_{lj}$ are calculated from the old volume δx by

$$\tilde{V}_{1j} = \delta x - ({}^{n}u_{1j-1/2} - {}^{n}u_{1j+1/2})\, \delta t$$

and

$$\tilde{V}_{2j} = \delta x - ({}^{n}u_{2j-1/2} - {}^{n}u_{2j+1/2})\, dt. \tag{10}$$

The artificial viscous pressure is

$$q_{1j} = -\frac{v_1\, {}^{n}M_{ij}}{(\delta x)^2}\,({}^{n}u_{1j+1/2} - {}^{n}u_{1j-1/2})$$

and

$$q_{2j} = -\frac{v_2\, {}^{n}M_{2j}}{(\delta x)^2}\,({}^{n}u_{2j+1/2} - {}^{n}u_{2j-1/2}). \tag{11}$$

If any q_{1j} is calculated less than zero we set it equal to zero. To obtain new velocities at this stage, we solve the two equations of momentum simultaneously. To simplify the mathematical expressions, we define "bar" velocities by writing

$$\begin{aligned}
\bar{u}_{1j+1/2} &= {}^{n}u_{1j+1/2} + \frac{({}^{n}\theta_{1j} + {}^{n}\theta_{1j+1})\,\delta t}{2\,{}^{n}\bar{M}_{1j+1/2}}\,({}^{n}p_j - {}^{n}p_{j+1}) \\
&\quad + \frac{\delta t}{{}^{n}\bar{M}_{1j+1/2}}\,({}^{n}q_{1j} - {}^{n}q_{1j+1}), \\
\bar{u}_{2j+1/2} &= {}^{n}u_{2j+1/2} + \frac{({}^{n}\theta_{2j} + {}^{n}\theta_{2j+1})\,\delta t}{2\,{}^{n}\bar{M}_{2j+1/2}}\,({}^{n}p_j - {}^{n}p_{j+1}) \\
&\quad + \frac{\delta t}{{}^{n}\bar{M}_{2j+1/2}}\,({}^{n}q_{2j} - {}^{n}q_{2j+1}).
\end{aligned} \tag{12}$$

If ${}^{n}\bar{M}_{lj+1/2} = 0$, then we set $\bar{u}_{lj+1/2} = 0$. We calculate the drag function according to

$$K_{j+1/2} = \frac{3C_{\mathrm{D}}\, {}^{n}\bar{M}_{2j+1/2}}{16 r_1\, \delta x}\,({}^{n}\theta_{1j} + {}^{n}\theta_{1j+1})\,|{}^{n}u_{1j+1/2} - {}^{n}u_{2j+1/2}| + 10^{-7}. \tag{13}$$

The small artificial addition 10^{-7} to the expression for K is present to prevent the occurrence of indefinites in the solution for the velocities when the edge mass ${}^{n}\bar{M}_{2j+1/2}$ is zero.

We now introduce "tilde" velocities ($\tilde{u}_{l2j+1/2}$), which must be modified in the next phase of the calculational cycle to take particle transport into account. They are therefore not the final updated velocities. These "tilde" velocities are given by the simultaneous solution of the two momentum equations,

$$\tilde{u}_{1j+1/2} = \bar{u}_{1j+1/2} + \frac{K_{j+1/2}\,\delta x \delta t}{\bar{M}_{1j+1/2}}\,(\tilde{u}_{2j+1/2} - \tilde{u}_{1j+1/2})$$

and

$$\tilde{u}_{2j+1/2} = \bar{u}_{2j+1/2} + \frac{K_{j+1/2}\delta x\delta t}{\bar{M}_{2j+1/2}}(\tilde{u}_{1j+1/2} - \tilde{u}_{2j+1/2}).$$

The solution of these equations is

$$\tilde{u}_{1j+1/2} = \frac{{}^n\bar{M}_{1j+1/2}\,{}^n\bar{M}_{2j+1/2}\bar{u}_{1j+1/2} + K_{j+1/2}\delta x\delta t({}^n\bar{M}_{1j+1/2}\bar{u}_{1j+1/2} + {}^n\bar{M}_{2j+1/2}\bar{u}_{2j+1/2})}{{}^n\bar{M}_{1j+1/2}\,{}^n\bar{M}_{2j+1/2} + K_{j+1/2}\delta x\delta t({}^n\bar{M}_{1j+1/2} + {}^n\bar{M}_{2j+1/2})}$$

and

$$\tilde{u}_{2j+1/2} = \frac{{}^n\bar{M}_{1j+1/2}\,{}^n\bar{M}_{2j+1/2}\bar{u}_{2j+1/2} + K_{j+1/2}\delta x\delta t({}^n\bar{M}_{1j+1/2}\bar{u}_{1j+1/2} + {}^n\bar{M}_{2j+1/2}\bar{u}_{2j+1/2})}{{}^n\bar{M}_{1j+1/2}\,{}^n\bar{M}_{2j+1/2} + K_{j+1/2}\delta x\delta t({}^n\bar{M}_{1j+1/2} + {}^n\bar{M}_{2j+1/2})}. \quad (14)$$

We perform an iteration to obtain the new locally equilibrated pressures. Using volume conservation and the equations of state, we solve the following three equations to obtain a first guess for equilibrium pressure and volume fractions. With $a_2 = 0$ (no "stiffening" in the gas) we have

$$p_j = a_1^2\left(\frac{\rho'_{1j}}{\theta_{1j}} - \rho_{01}\right) + (\gamma_1 - 1)\frac{\rho'_{1j}}{\theta_{1j}}\tilde{I}_{1j},$$

$$p_j = (\gamma_2 - 1)\frac{\rho'_{2j}}{\theta_{2j}}\tilde{I}_{2j},$$

and

$$\theta_{1j} + \theta_{2j} = 1.$$

$\tilde{I}_{1j}$ is an approximation to the new specific internal energy that is subsequently modified to take into account dissipation and conduction. The solution of these equations represents a first guess because the internal energies do not include the compressional work that is associated with the changes in volume calculated in this phase. The new values of $\tilde{I}_{1j}$ and $\tilde{I}_{2j}$ are then calculated from the new pressures and volume fractions,

$$\tilde{I}_{1j} = {}^nI_{1j} - \frac{\left({}^{n+1}p_j + \dfrac{{}^nq_{1j}}{{}^{n+1}\theta_{1j}}\right)}{{}^nM_{1j}}({}^{n+1}\tilde{V}_{1j}\,{}^{n+1}\theta_{1j} - \delta x\,{}^n\theta_{1j})$$

and

$$\tilde{I}_{2j} = {}^nI_{2j} - \frac{\left({}^{n+1}p_j + \dfrac{{}^nq_{2j}}{{}^{n+1}\theta_{2j}}\right)}{{}^nM_{2j}}({}^{n+1}\tilde{V}_{2j}\,{}^{n+1}\theta_{2j} - \delta x\,{}^n\theta_{2j}). \quad (15)$$

If ${}^nM_{1j}$ or ${}^nM_{2j}$ is zero we set the corresponding $\tilde{I}$ equal to zero. With these values of $\tilde{I}$ we repeat the whole equilibration. By examining a set of trial calculations, we have found that five repetitions produce satisfactory accuracy.

The final calculation in phase 1 is the inclusion of the drag-function dissipation in the specific internal energies. To derive an expression for the dissipation, we rewrite the momentum equations in the form

$${}^n\bar{M}_{1j+1/2}(\tilde{u}_{1j+1/2} - \bar{u}_{1j+1/2}) = K_{j+1/2}\delta x\delta t(\tilde{u}_{2j+1/2} - \tilde{u}_{1j+1/2})$$

and

$${}^n\bar{M}_{2j+1/2}(\tilde{u}_{2j+1/2} - \bar{u}_{2j+1/2}) = K_{j+1/2}\delta x\delta t(\tilde{u}_{1j+1/2} - \tilde{u}_{2j+1/2}). \tag{16}$$

Multiplying the first equation by $\frac{1}{2}(\tilde{u}_{1j+1/2} + \bar{u}_{1j+1/2})$, the second by $\frac{1}{2}(\tilde{u}_{2j+1/2} + \bar{u}_{2j+1/2})$, adding, and rearranging, we obtain the change in kinetic energy, δKE_{12}, that results from a coupling of the two fields. In expanding the expression we neglect terms of order $(\delta t)^2$, with the result

$$\delta KE_{12} = -K_{j+1/2}\delta x\delta t(\tilde{u}_{2j+1/2} - \tilde{u}_{1j+1/2})^2. \tag{17}$$

The change in specific internal energy $\delta I_{j+1/2}$ that results from this dissipation of kinetic energy is

$$\delta I_{j+1/2} = \frac{-\delta KE_{12}}{{}^n\bar{M}_{1j+1/2} + {}^n\bar{M}_{2j+1/2}}. \tag{18}$$

We add this amount to the "tilde" specific internal energies, $\tilde{I}_{lj}$ and $\tilde{I}_{lj+1}$ $(l = 1, 2)$.

In phase 2 we calculate the convective contributions to the equations. We begin by calculating the total momentum in the edge zones and the total internal energy in the cell-centered zones.

$${}^nY_{1j+1/2} = {}^n\bar{M}_{1j+1/2}\tilde{u}_{1j+1/2},$$
$${}^n\bar{Y}_{2j+1/2}{}^n\bar{M}_{2j+1/2}\tilde{u}_{2j+1/2},$$
$${}^nE_{1j} = M_{1j}\tilde{I}_{1j}.$$

and

$${}^nE_{2j} = M_{2j}\tilde{I}_{2j}. \tag{19}$$

To move the particles we first must locate them in the Eulerian mesh. We define an index ${}^nj_c$ that corresponds to the cell in which the particle is located at the end of the previous computational cycle. For material l we have

$${}^nj_c = 2 + \text{Integer}\left(\frac{{}^nx_{li}}{\delta x}\right). \tag{20}$$

We now determine the location of its Eulerian interfaces.

$$x_{jR} = ({}^{n}j_c - 1)\,\delta x$$

and

$$x_{jL} = x_{jR} - \delta x, \tag{21}$$

where the right interface of ${}^{n}j_c$ is x_{jR} and the left interface is x_{jL}. Similarly, we define an integer number ${}^{n}j_e$ that identifies each zone centered on a cell interface.

$${}^{n}j_e = \text{Integer}\left(\frac{{}^{n}x_{li}}{\delta x} + \frac{3}{2}\right). \tag{22}$$

Using a linear interpolation for the particle velocity we calculate a new location for the particle. To simplify the notation we replace ${}^{n}j_c$ with c.

$${}^{n+1}x_{li} = {}^{n}x_{li} + \frac{\delta t}{\delta x}\left[(x_{jR} - {}^{n}x_{li})\,u_{lc-1/2} + ({}^{n}x_{li} - x_{jL})\,u_{lc+1/2}\right]. \tag{23}$$

The quantity ${}^{n+1}x_{li}$ is the new particle location for the current computational cycle. Using Eqs. 20 and 22 we update j_c and j_e to determine if any cell boundaries have been traversed.

If ${}^{n+1}j_c$ does not equal ${}^{n}j_c$, the particle has crossed from one cell-centered zone to another. Appropriate adjustments are made in the internal energy and mass of the associated zones. If ${}^{n+1}j_e$ does not equal ${}^{n}j_e$ the particle has crossed an edge zone, so we adjust the momenta and edge masses. In addition, we modify the internal energy of the appropriate cell-centered zones to allow for the resulting dissipation. To treat the change in internal energy correctly we must relate the edge boundary crossed by the particle to the cell-centered zone containing that boundary.

The dissipation for this process can be investigated by a detailed examination of the loss of kinetic energy, which is of the following form for particles of material l

$$\delta KE = -\frac{1}{2}\frac{m_l\,{}^{n}\bar{M}_{lj+3/2}}{m_l + \bar{M}_{lj+3/2}}(\tilde{u}_{lj+3/2} - \tilde{u}_{lj+1/2})^2. \tag{24}$$

The above expression is negative definite as it must be. The dissipation term is

$$\delta E_d = -\delta KE. \tag{25}$$

We partition this energy equally between the calculational cell and the neighboring cell if the latter has non-zero mass; othewise it is added only to the computational cell. The edge masses are treated in the same manner as the cell-centered masses.

We calculate the new location of each reserve particle by

$$^{n+1}x_{2l} = {}^{n}x_{2l} + u_{2R}\,\delta t. \tag{26}$$

If the particle has crossed the mesh boundary, we make appropriate modifications in particle numbers, total internal energy and cell- and edge-centered mass.

In the final stage of the phase 2 calculation, we use our newly determined momenta, internal energies, cell-centered masses, and edge masses to obtain updated velocities and specific internal energies. If the edge mass of l is nonzero for a particular zone, we calculate the velocity by

$$^{n+1}u_{lj+1/2} = \frac{Y_{lj+1/2}}{^{n+1}\bar{M}_{lj+1/2}}. \tag{27}$$

If one material is absent from an edge zone, we set the velocity of that material equal to the velocity of the other material.

To obtain the specific internal energies we divide the total internal energy of a cell-centered zone by its total mass.

$$\tilde{I}_{lj} = \frac{E_{lj}}{^{n+1}M_{lj}}. \tag{28}$$

If no mass of l is present in a zone, we set the specific internal energy of that material to zero. At this point the specific internal energies are not final for this computational cycle, so we continue to designate them as "tilde" quantities.

In phase 3 we calculate the contribution of the heat diffusion term to the specific internal energies. The difference form of the second-order partial derivative in the heat diffusion term uses the lesser of the two cell-centered masses adjacent to the interface under consideration, thus avoiding excessive flux to or from a cell with small mass. We refer to these masses as $M_{l\mathrm{R}}$ and $M_{l\mathrm{L}}$. The new specific internal energies are given by

$$^{n+1}I_{lj} = \tilde{I}_{lj} + \frac{\xi_l\,\delta t}{^{n+1}M_{lj}(\delta x)^2}\,[M_{l\mathrm{R}}(\tilde{I}_{lj+1} - \tilde{I}_{lj}) - M_{l\mathrm{L}}(\tilde{I}_{lj} - \tilde{I}_{lj-1})]. \tag{29}$$

If $^{n+1}M_{lj}$ equals zero we set $^{n+1}I_{lj}$ equal to zero. With the three phases of the computational cycle complete, we recalculate pressures and volume fractions based on the new specific internal energies.

IV. Numerical Accuracy

Although the accuracy of the calculations is very difficult to demonstrate in general, we have used two tests to indicate whether the results represent reliable solutions of the differential equations. One test is the calculation of a selected problem with three different degrees of resolution. The configuration used in this comparison is the one described in Section I, a fragmented metal disc with gas regions on the leading and trailing edges. In the calculation we used 300, 90 and 30 cells for the fine, intermediate, and coarse meshes, respectively. The results shown in Fig. 5 indicate relatively little difference among the three calculations, although there is increased sharpness of the interfaces with finer resolution. The second test, discussed below, is a study of the propagation of weak signals through an initially mixed region.

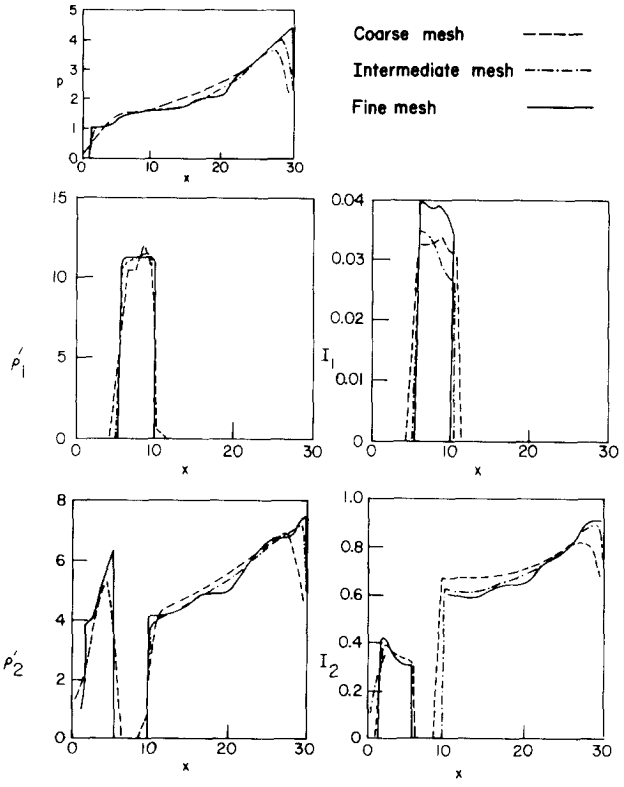

FIG. 5. Effect of zone size: PICM predictions at a selected time of pressure, p; of the macroscopic densities, ρ_1' and ρ_2', in the fragmented metal and in the gas, respectively; and of the specific internal energy, I_1 and I_2, in the fragmented metal and in the gas, respectively.

V. Sound Speed in a Mixture

According to the classical theory given by Wood [7], a low-amplitude signal propagates through a mixture of strongly coupled materials with a speed given by the following equation.

$$C^2 = \frac{C_1^2 C_2^2 \rho_1 \rho_2}{[\theta_1 C_2^2 \rho_2 + \theta_2 C_1^2 \rho_1][\theta_1 \rho_1 + \theta_2 \rho_2]}, \tag{30}$$

in which C_1 and C_2 are the pure-material sound speeds for the two components of the mixture. We consider first the case in which the ratio of the microscopic densities between the two materials is 11 to 1, with a set of material properties and initial conditions as given in Tables I and II, for which $C_1 = 1.03$ and $C_2 = 1.29$. The mixture sound speed computed by the above equation is $C = 0.74$. To directly proof-test the numerical method for this type of example requires computer calculations for the propagation of a very weak disturbance through the mixture. It has been demonstrated previously, however, that PIC calculations [8] can develop severe fluctuations when the Mach number of the flow is much smaller than 1. To test the numerical methodology we have performed a series of calculations, each with a weaker disturbance impressed onto the fluid mixture, and have extrapolated the results for comparison with the low-amplitude limit.

The configuration for the calculations is summarized in Tables II and III and consists of regions A and B, of which A contains the mixture and B the pure gas. In the pure gas we initiate a shock for each calculation, the strength of which is charac-

TABLE I

Material Properties

l	ρ_{0l}	γ_l	a_l	C_D	r_1
1	10.0	$\frac{5}{3}$	1.0	1.0	0.0001
2	0.0	$\frac{5}{3}$	0.0	—	—

TABLE II

Initial Conditions

Region	ρ'_{1j}	ρ'_{2j}	θ_{1j}	θ_{2j}	I_{1j}	I_{2j}	p_j	$u_{1j+1/2}$	$u_{2j+1/2}$
A	8.25	0.25	0.75	025	0.0	1.5	1.0	0.0	0.0
B	0.0	1.0	0.0	1.0	0.0	1.5	1.0	0.0	0.0

TABLE III

Calculation Mesh

Mach No.	δx	δt	j_1	$\bar{J}$	N_1	N_2	ν_1	ν_2	ξ_1	ξ_2
2.0	1.0	0.1	16	30	16	8	0.2	0.2	0.2	0.2
1.5	1.0	0.1	16	30	16	8	0.2	0.2	0.2	0.2
1.1	0.33	0.033	46	90	64	32	0.06	0.06	0.06	0.06

TABLE IV

Boundary Conditions

Mach No.	ρ'_{1J+2}	ρ'_{1J+2}	I_{1J+2}	I_{2J+2}	P_{J+2}	$u_{1J+3/2}$	$u_{2J+3/2}$
2.0	0.0	2.286	0.0	3.117	4.750	0.0	−1.452
1.5	0.0	1.174	0.0	2.242	2.562	0.0	−0.807
1.1	0.0	1.150	0.0	1.647	1.263	0.0	−0.185

terized by the Mach number, M, defined as the ratio of the shock speed to the sound speed in the undisturbed gas of region B. In Table IV we indicate the boundary conditions supplied to the right side of the system.

In each case we measure the transit time of the signal across A. For $M = 2.0$, a relatively coarse computational mesh produces sufficient resolution of the transmitted signal. In this case, a coarse mesh means 15 cells across the mixture region and particle densities of 16 and 8 for materials 1 and 2, respectively. We find that the calculation with $M = 1.1$ requires a finer mesh and higher particle densities to reduce the computational fluctuations associated with the "perturbed stagnation" of the materials, a difficulty that has always required special treatment in PIC-based methodologies. This calculation requires 45 cells across the mixture region and particle densities of 64 and 32 per cell for materials 1 and 2, respectively. The calculation with $M = 1.5$ also has computational fluctuations, albeit to a lesser degree. A plot of the three signal speeds is shown as a function of M in Fig. 6 together with the theoretical result for a weak signal ($M = 0$). The extrapolated result agrees closely with theory.

As a more stringent test, we have performed a similar set of calculations using a density ratio of 100 to 1. The pure-material sound speeds of the metal and the gas are C_1 and $C_2 = 1$, respectively. In this case, the mixture sound speed has the theoretical value $C = 0.2$, which is one-fifth of the sound speed in either material by itself. Again the extrapolation of the calculated results to $M = 0$ agrees closely with theory, as shown in Fig. 7.

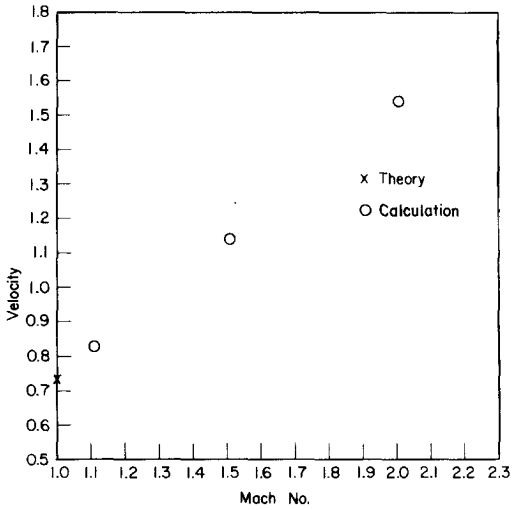

FIG. 6. Signal speed as a function of Mach number.

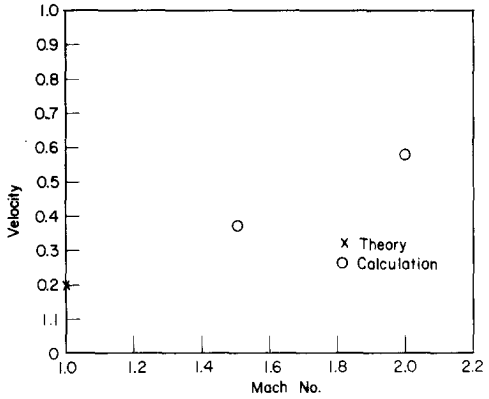

FIG. 7. Signal speed as a function of Mach number.

VI. CONCLUSIONS

We have developed a modified version of the PIC method by which the relative dynamics of a fragmented metal and a shocked gas can be calculated with both accuracy and efficiency. Test calculations show that the numerical procedure is capable of maintaining a sharp interface for circumstances that should be stable, and of allowing interpenetration for unstable interfaces. Additional tests demonstrate the capability for accurate calculation of sound signal propagation through a two-phase mixture. The principal application of the technique, described elsewhere [1], has been to investigate the shock compression of several interpenetrating materials, for which the numerical methodology succeeds even for high-density ratios.

REFERENCES

1. L. COOK, B. DEMUTH, AND H. HARLOW, "Multiphase Interpetation of Shocked Materials," Los Alamos Scientific Laboratory report LA-7578 (February 1979).
2. H. HARLOW AND A. A. AMSDEN, *J. Comput. Phys.* **17** (1975), 19–52.
3. A. A. AMSDEN, "The Particle-in-Cell Method for the Calculation of the Dynamics of Compressible Fluids," Los Alamos Scientific Laboratory report LA-3466 (February 1966).
4. H. HARLOW AND A. A. AMSDEN, *J. Comput. Phys.* **18** (1975), 440–464.
5. A. A. AMSDEN AND F. H. HARLOW, "K-TIF: A Two-Fluid Computer Program for Downcomer Flow Dynamics," Los Alamos Scientific Laboratory report LA-6994 (January 1978).
6. H. HARLOW AND A. A. AMSDEN, "Fluid Dynamics," Los Alamos Scientific Laboratory report LA-4700 (June 1971).
7. A. B. WOOD, "A Textbook of Sound," Bell, London, 1960.
8. H. HARLOW, "Two-Dimensional Hydrodynamic Calculations," Los Alamos Scientific Laboratory report LA-2301 (April 1959).